Impact of Vector Ordering Strategies on Morphological Unmixing of Remotely Sensed Hyperspectral Images

Antonio Plaza and Javier Plaza
Hyperspectral Computing Laboratory
Department of Technology of Computers and Communications
University of Extremadura, Avda. de la Universidad s/n, E-10071 Cáceres, SPAIN
URL: http://www.umbc.edu/rssipl/people/aplaza – E-mail: {aplaza,jplaza}@unex.es

Abstract

Hyperspectral imaging is a new technique in remote sensing that generates hundreds of images, corresponding to different wavelength channels, for the same area on the surface of the Earth. In previous work, we have explored the application of morphological operations to integrate both spatial and spectral responses in hyperspectral data analysis. These operations rely on ordering pixel vectors in spectral space, but there is no unambiguous means of defining the minimum and maximum values between two vectors of more than one dimension. Our original contribution in this paper is to examine the impact of different vector ordering strategies on the definition of multi-channel morphological operations. Our focus is on morphological unmixing, which decomposes each pixel vector in the hyperspectral scene into a combination of pure spectral signatures (called endmembers) and their associated abundance fractions, allowing sub-pixel characterization. Experiments are conducted using real hyperspectral data sets collected by NASA/JPL's Airborne Visible Infra-Red Imaging Spectrometer (AVIRIS) system.

1 Introduction

Hyperspectral imaging is concerned with the measurement, analysis, and interpretation of spectra acquired from a given scene (or specific object) at a short, medium or long distance by an airborne or satellite sensor [3]. The concept of hyperspectral imaging originated at NASA's Jet Propulsion Laboratory in California, which developed instruments such as the Airborne Imaging Spectrometer (AIS), then called AVIRIS, for Airborne Visible Infra-Red Imaging Spectrometer [4]. This system is now able to cover the wavelength region

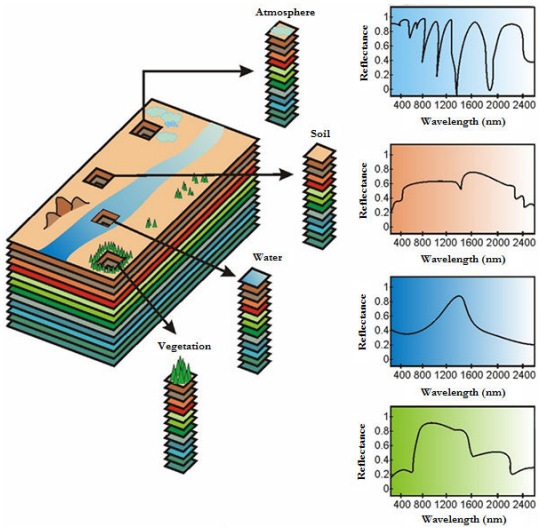

Figure 1. Hyperspectral imaging concept

from 0.4 to 2.5 μm using more than two hundred spectral channels, at nominal spectral resolution of 10 nm. As a result, each pixel vector collected by a hyperspectral instrument can be seen as a *spectral signature* or *fingerprint* of the underlying materials within the pixel (see Fig. 1).

Spectral mixture analysis has been an alluring exploitation goal since the earliest days of hyperspectral imaging [5]. No matter the spatial resolution, in natural environments the spectral signature for a nominal pixel is invariably a mixture of the signatures of the various materials found within the spatial extent of the ground instantaneous field view [8]. In hyperspectral imagery, the number of spectral bands usually exceeds the number of pure spectral components, called *endmembers* in hyperspectral analysis terminology [7], and the unmixing problem is cast in terms of an over-determined sys-

1051-4651/10 $26.00 © 2010 IEEE
DOI 10.1109/ICPR.2010.1072

tem of equations in which, given the correct set of endmembers allows determination of the actual endmember abundance fractions through a numerical inversion process. Since each observed spectral signal is the result of an actual mixing process, the driving abundances must obey two constraints [2]. First, all abundances must be non-negative. Second, the sum of abundances for a given pixel must be unity.

In previous work, we have explored the application of multi-channel morphological operations to integrate both spatial and spectral responses in spectral mixture analysis of hyperspectral images [6]. A simple approach to multi-channel morphology consists in applying single-channel morphological techniques to each channel separately [9]. However, with this *marginal* approach there is a possibility for loss or corruption of information of the image due to the probable fact that new spectral constituents –not present in the original image– may be created as a result of processing the channels separately. An alternative way to approach the problem of multi-channel morphology is to treat the data at each pixel as a vector. Unfortunately, there is no unambiguous means of defining the minimum and maximum values between two vectors of more than one dimension, and thus it is important to define an appropriate arrangement of vectors in the selected vector space.

In this work, we examine the impact of different vector ordering strategies on the definition of multi-channel morphological operations for spectral unmixing of remotely sensed hyperspectral data. Our ultimate goal is to provide specific recommendations on best practice when defining vector-based multi-channel morphological operations. The remainder of this paper is organized as follows. Section 2 describes the approach followed for extension of morphological operations to hyperspectral imagery. Section 3 discusses different vector ordering strategies. Section 4 describes a morphological endmember extraction algorithm based on extended morphological operations. Section 5 provides an experimental evaluation of the considered endmember extraction algorithm, implemented using different ordering strategies, along with a comparison to other existing endmember extraction using real hyperspectral datasets collected by the 224-channel NASA's AVIRIS system. Section 6 concludes with some summarizing points and hints at plausible future research.

2 Extended mathematical morphology

Mathematical morphology is a theory for spatial structure analysis that was established by introducing fundamental operators applied to two sets [9]. A set is processed by another one having a carefully selected shape and size, known as the structuring element (SE). The two basic operations of mathematical morphology are erosion and dilation [9]. In grayscale morphology, these operators can be interpreted by viewing the image data as an imaginary topographic relief in which the brighter the gray tone, the higher the corresponding elevation. With this assumption in mind, morphological operations can be interpreted as the result of sliding a SE over the topographical relief, so that the SE defines the new (dilated or eroded) scene based on its spatial properties.

Extension of morphological operators to multi-channel data such as hyperspectral imagery with hundreds of spectral channels is not straightforward. A simple approach consists in applying grayscale morphology techniques to each channel separately, an approach that has been called *marginal morphology* in the literature [9]. However, the marginal approach is often unacceptable in remote sensing applications because, when morphological techniques are applied independently to each image channel, analysis techniques are subject to the well-known problem of *false colors*; that is, it is very likely that new spectral constituents (not present in the original hyperspectral image) may be created as a result of processing the channels separately. An alternative (and perhaps more appropriate) way to approach the problem of multi-channel morphology is to treat the data at each pixel as a vector [6]. Unfortunately, there is no unambiguous means of defining the minimum and maximum values between two vectors of more than one dimension, and thus it is important to define an appropriate arrangement of vectors in the selected vector space.

Let us assume that $\mathbf{f}$ is a hyperspectral image defined on the N-dimensional continuous space, where N is the number of spectral channels. Similarly, let us assume that $\mathbf{f}(x, y)$ denotes the pixel vector at spatial coordinates (x, y). The pixel vectors in the spatial neighborhood of $\mathbf{f}(x, y)$ defined by a SE denoted by K are represented by $\mathbf{f}(s, t)$ so that $(s, t) \in K$. With the above definitions in mind, the extended erosion $\mathbf{f} \ominus K$ can be defined as follows [6]:

$$(\mathbf{f} \ominus K)(x, y) = min_{(s,t)\in K}\{\mathbf{f}(x + s, y + t)\}. \quad (1)$$

On the other hand, the extended dilation $\mathbf{f} \oplus K$ can be defined as follows [6]:

$$(\mathbf{f} \oplus K)(x, y) = max_{(s,t)\in K}\{\mathbf{f}(x - s, y - t)\}. \quad (2)$$

As shown by Eqs. (1) and (2), multi-channel morphology is based on the definition of a vector ordering strategy able to determine a maximum and an minimum given a set of pixel vectors.

3 Vector ordering strategies

Several classic strategies have been defined in the literature to order vectors in N-dimensional space. If we assume that $\mathbf{f}(x,y)$ and $\mathbf{f}(x',y')$ denote two pixel vectors with $\mathbf{f}(x,y) = [f_1(x,y), \cdots, f_N(x,y)]$ and $\mathbf{f}(x',y') = [f_1(x',y'), \cdots, f_N(x',y')]$, respectively, the following strategies can be applied:

- In marginal ordering (M-ordering), each pair of observations $f_i(x,y)$ and $f_i(x',y')$ is ordered independently along each of the N channels.
- In conditional ordering (C-ordering), the pixel vectors are initially ordered according to the ordered values of one of their components, e.g. the first component, $f_1(x,y)$ and $f_1(x',y')$. As a second step, vectors that have the same value for the first component are ordered according to the ordered values of another component, e.g. the second component, $f_2(x,y)$ and $f_2(x',y')$, and so on.

It should be noted that pixel vectors in remotely sensed images are usually considered as entire spectral signatures (see Fig. 1) in which all channels can provide relevant information. In addition, the spectral signatures may be affected by atmospheric and illumination interferers, which may introduce fluctuations in the amount of energy collected by the sensor at the different wavelength channels. To address these properties, a different ordering strategy that considers the full spectral signature *as a whole* (D-ordering) is introduced. This strategy utilizes a cumulative distance between one particular pixel vector $\mathbf{f}(x,y)$ and all the pixel vectors in the spatial neighborhood given by a SE denoted by K as follows [6]:

$$C_K(\mathbf{f}(x,y)) = \sum_{(s,t)\in K} \text{SAD}(\mathbf{f}(x,y), \mathbf{f}(s,t)), \qquad (3)$$

where SAD is the spectral angle distance [2]. The SAD between $\mathbf{f}(x,y)$ and $\mathbf{f}(s,t)$ is given by the following expression:

$$\text{SAD}(\mathbf{f}(x,y), \mathbf{f}(s,t)) = \cos^{-1}\left(\frac{\mathbf{f}(x,y)\cdot\mathbf{f}(s,t)}{\|\mathbf{f}(x,y)\|\cdot\|\mathbf{f}(s,t)\|}\right). \qquad (4)$$

As a result, $C_K(\mathbf{f}(x,y))$ is given by the sum of SAD scores between $\mathbf{f}(x,y)$ and every other pixel vector in the K-neighborhood. The SAD measurement is invariant in the multiplication of the input vectors by constants and, consequently, is invariant to unknown multiplicative scalings that may arise due to differences in illumination and sensor observation angle [2].

4 Morphological endmember extraction

Based on the multi-channel operations of erosion and dilation described in section 2, we have developed an algorithm for automated morphological endmember extraction (AMEE) [6]. The inputs to the algorithm are the full hyperspectral data cube **f**, a SE denoted by *K*, a maximum number of algorithm iterations I_{max}, and a number of endmembers to be extracted, *p*. A step-by-step description of the algorithm follows:

1. Set $i = 1$ and initialize a morphological eccentricity index [6], denoted by $\text{MEI}(x,y) = 0$, for each pixel $\mathbf{f}(x,y)$ in the original image.
2. Move *K* through all the pixels of the image, defining a local spatial search area around each pixel $\mathbf{f}(x,y)$, and update the MEI at each spatial location (x,y) using the following expression:
$$\text{MEI}(x,y) = \text{SAD}[(\mathbf{f}\ominus K)(x,y), (\mathbf{f}\oplus K)(x,y)] \qquad (5)$$
3. Set $i = i+1$. If $i = I_{max}$, then label the p distinct pixel vectors with higher MEI scores as the final endmembers. Otherwise, replace the original image with its dilation using *K* and go to step 2.

5 Experimental results

In this section, we evaluate the impact of using different vector ordering strategies in the definition of multi-channel morphological operations adopted by the AMEE algorithm, and further compare the obtained results with those provided by other classic algorithms for endmember extraction in the literature, such as the pixel purity index (PPI) [1] and N-FINDR [10].

The image data set used in experiments was collected by NASA Jet Propulsion Laboratory's AVIRIS system over the Cuprite mining district in Nevada. The data set[1] consists of 614×512 pixels and 224 bands in the wavelength range 0.4–2.5 μm (137 MB in size). It is atmospherically corrected and available in reflectance units. The Cuprite site has been extensively mapped by the U.S. Geological Survey (USGS) in the last twenty years, and there is extensive ground-truth information available, including a library of mineral signatures collected on the field[2].

Table 1 shows the SAD scores (in degrees) between the endmembers in the final endmember set (extracted by different endmember extraction algorithms) and their corresponding spectral signatures in the USGS

[1] Online: http://aviris.jpl.nasa.gov/html/aviris.freedata.html
[2] Online: http://speclab.cr.usgs.gov/spectrallib.html

Table 1. SAD scores (degrees) between USGS mineral spectra and their corresponding endmembers produced by several endmember extraction algorithms.

USGS	Spectral methods:		Spatial-spectral AMEE method:		
signature	PPI	N-FINDR	(M-ord.)	(C-ord.)	(D-ord.)
Alunite	10.12^o	9.96^o	11.05^o	7.81^o	4.81^o
Buddingt.	8.23^o	7.71^o	9.34^o	9.12^o	4.21^o
Calcite	12.36^o	12.08^o	13.32^o	12.55^o	9.54^o
Kaolinite	13.05^o	13.27^o	13.46^o	11.19^o	8.74^o
Muscovite	6.35^o	5.24^o	8.44^o	7.69^o	4.61^o

library. We individually optimized the input parameters for each endmember extraction algorithm to make sure that the best performance of each considered algorithm with the AVIRIS Cuprite scene is reported in Table 1. In order to display the results in a more effective manner, we only report the SAD score associated to the most similar spectral endmember (out of $p = 15$ endmembers obtained for each algorithm combination, where this value was determined by using the virtual dimensionality concept in [2]) with regards to its corresponding USGS signature. It is important to emphasize that smaller SAD values indicate higher spectral similarity.

As shown by Table 1, the AMEE (implemented with D-ordering) resulted in the largest number of minimal SAD values (displayed in bold typeface in the table) among all considered combinations. Quite opposite, the AMEE implemented with M-ordering and C-ordering produced endmembers which were less similar, spectrally, with regards to reference USGS signatures. Even though PPI and N-FINDR are spectral-based methods that do not incorporate the spatial information in the search for endmembers, their performance can be superior to that of the spatial-spectral AMEE if an inappropriate vector ordering strategy is used to define extended morphological operations.

The considered endmember extraction algorithms have also been evaluated from the viewpoint of their capacity to produce high-quality abundance estimations for geological features in the Cuprite mining district. This has been done by estimating the fractional abundance of endmembers provided by PPI, N-FINDR and AMEE using the standard linear spectral unmixing (LSU) algorithm for abundance estimation [2]. In all cases, we tested unconstrained versus fully constrained versions (i.e., with sum-to-one and non-negativity restrictions) of the LSU. Although ground-truth information on endmember fractional abundances is very difficult to obtain in real-world scenarios, our quantitative experiments demonstrated that the use of AMEE (implemented with D-ordering) resulted in very few negative abundance estimations. In contrast, a more significant fraction of negative abundances was obtained when using all other tested methods (in particular, the AMEE implemented using M-ordering and C-ordering).

6 Conclusions and future research

In this work, we have explored the impact of different vector ordering strategies on the definition of multichannel morphological operations for spectral unmixing of remotely sensed hyperspectral images. Our experiments indicate that a physically meaningful strategy that considers spectral angle distances between full spectral signatures (D-ordering) provides superior results to those obtained using M-ordering and C-ordering strategies. A spatial-spectral endmember extraction algorithm implemented using D-ordering also provides higher quality endmembers and fractional abundance estimations than other classic methods that only use spectral information for the unmixing stage. Further experiments with additional distance metrics and scenes should be conducted in order to fully substantiate the results presented in this paper.

References

[1] J. W. Boardman, F. A. Kruse, and R. O. Green. Mapping target signatures via partial unmixing of AVIRIS data. *Proc. JPL Earth Science Workshop*, pages 23–26, 1995.

[2] C.-I. Chang. *Hyperspectral Imaging: Techniques for Spectral Detection and Classification*. Kluwer, 2003.

[3] A. F. H. Goetz, G. Vane, J. E. Solomon, and B. N. Rock. Imaging spectrometry for Earth remote sensing. *Science*, 228:1147–1153, 1985.

[4] R. O. Green et al. Imaging spectroscopy and the airborne visible/infrared imaging spectrometer (AVIRIS). *Remote Sensing of Environment*, 65(3):227–248, 1998.

[5] A. Plaza et al. Recent advances in techniques for hyperspectral image processing. *Remote Sensing of Environment*, 113:110–122, 2009.

[6] A. Plaza, P. Martinez, R. Perez, and J. Plaza. Spatial/spectral endmember extraction by multidimensional morphological operations. *IEEE Transactions on Geoscience and Remote Sensing*, 40(9):2025–2041, 2002.

[7] A. Plaza, P. Martinez, R. Perez, and J. Plaza. A quantitative and comparative analysis of endmember extraction algorithms. *IEEE Transactions on Geoscience and Remote Sensing*, 42(3):650–663, 2004.

[8] J. Plaza, A. Plaza, R. Perez, and P. Martinez. On the use of small training sets for neural network-based characterization of mixed pixels in remotely sensed hyperspectral images. *Pattern Recognition*, 42:3032–3045, 2009.

[9] P. Soille. *Morphological image analysis: Principles and applications*. Springer, 2003.

[10] M. E. Winter. N-FINDR: An algorithm for fast autonomous spectral endmember determination in hyperspectral data. *Proc. SPIE*, 3753:266–277, 1999.